Probabilistic multiconstraints optimization of cooling channels in ceramic matrix composites

Hamid Ghasemi[**1], Pierre Kerfriden[2], Stéphane P. A. Bordas[2,3], J. Muthu[4],Goangseup Zi[5], Timon Rabczuk*[1,5]**

[1] Institute of Structural Mechanics, Bauhaus University Weimar, Marienstraße 15, 99423 Weimar, Germany
[2] Institute of Mechanics and Advanced Materials, Cardiff University, Cardiff CF 24 3AA, UK
[3] Faculté des Sciences, de la Technologie et de la Communication, Université du Luxembourg, Campus Kirchberg, 6, rue Coudenhove-Kalergi, L-1359, Luxembourg
[4] School of Mechanical, Industrial and Aeronautical Eng., Uni. of the Witwatersrand, WITS 2050, S. Africa
[5] School of Civil, Environmental and Architectural Eng., Korea University, Seoul, S. Korea

Abstract

This paper presents a computational reliable optimization approach for internal cooling channels in Ceramic Matrix Composite (CMC) under thermal and mechanical loadings. The algorithm finds the optimal cooling capacity of all channels (which directly minimizes the amount of coolant needed). In the first step, available uncertainties in the constituent material properties, the applied mechanical load, the heat flux and the heat convection coefficient are considered. Using the Reliability Based Design Optimization (RBDO) approach, the probabilistic constraints ensure the failure due to excessive temperature and deflection will not happen. The deterministic constraints restrict the capacity of any arbitrary cooling channel between two extreme limits. A "series system" reliability concept is adopted as a union of mechanical and thermal failure subsets. Having the results of the first step for CMC with uniformly distributed carbon (C-) fibers, the algorithm presents the optimal layout for distribution of the C-fibers inside the ceramic matrix in order to enhance the target reliability of the component. A sequential approach and B-spline finite elements have overcome the cumbersome computational burden. Numerical results demonstrate that if the mechanical loading dominates the thermal loading, C-fibers distribution can play a considerable role towards increasing the reliability of the design.

Keywords: A. Ceramic-matrix composites (CMCs); B. Thermomechanical; C. Finite element analysis (FEA); C. Statistical properties/methods; Optimization

1. Introduction

The main disadvantage of monolithic ceramics is their low fracture toughness. Thus, carbon fibers are added to increase their damage tolerance while maintaining other advantages (for instance lower

---

*Corresponding Author: Tel: (+49)3643-584511, E-Mail: timon.rabczuk@uni-weimar.de
**Corresponding Author: E-Mail: hamid.ghasemi@uni-weimar.de

density and higher maximum operating temperature compared to metals or high erosion and corrosion resistance).

As a common reinforcing ingredient, C-fibers degrade in an oxidizing atmosphere beyond 450 degrees Celsius [1]. Although multilayer protection coatings hinder degradation to a degree, the coating process may itself result in formation of interphasial cracks. Preventing high temperature zones in the component might be a better solution. Such a solution however calls for a multidisciplinary approach accounting for material selection, coating and internal cooling design.

This paper presents a computational framework for an efficient and reliable internal cooling network for a typical component made of CMC. Although some attempts to optimize internal cooling system of a monotonic metallic turbine blade exist, the currently known approaches are limited to using heuristic optimization methods, particularly Genetic Algorithm (GA) which is computationally expensive. For example, Dennis et al. [2] used parallel genetic algorithm to optimize locations and discrete radii of a large number of small circular cross-section coolant passages. Nagaiah and Geiger [3] used NSGA-II as a multiobjective evolutionary algorithm optimizing the rib design inside a 2D cooling channel of a gas turbine blade. In both works an external commercial finite element package is used for the thermal analysis.

Regardless of the optimization technique, another major drawback of current methods is their deterministic nature. Actual characteristics of a composite material (including CMC) involve many uncertainties. These emanate from a variety of sources such as constituent material properties, manufacturing and process imperfections, loading conditions and geometry (a classification is presented in [4]). Neglecting the role of uncertainties in composite materials might result in either unsafe or unnecessary conservative design. This research focuses not only on optimal but also on reliable design of a typical internal cooling network within a CMC using a non-heuristic method and accounting for uncertainties.

We take advantage of sequential optimization approach [5] and propose a two stage optimization process in which the stages are sequentially linked to each other. In the first stage, it is assumed that C-fibers are uniformly distributed in the ceramic matrix. Then by using RBDO, the outputs of the first stage which are optimal capacities of the cooling channels, are exported into the next stage. In the second stage, the optimizer takes these inputs and uses the adjoint sensitivity technique adopted for the coupled elastic and thermal fields and eventually provides an optimal distribution of the C-fibers within the design domain in order to enhance the target reliability of the component.

The remainder of this paper is organized as follows: In Section 2 and Section 3, the thermoelastic finite element formulations and structural reliability concept are briefly discussed. The optimization methodology is explained in Section 4. Afterwards, case studies in Section 5 and concluding remarks in Section 6 are presented.

2. Thermoelastic formulation

The steady-state governing equation and boundary conditions for a temperature field in a 2D isotropic solid with domain Ω and boundary Γ are [6]

$$\left(k_{ij}\theta_{,j}\right)_{,i} + Q = 0 \qquad \text{in } \Omega \tag{1}$$

$$\theta = \theta_{\Gamma} \qquad \text{on } \Gamma_1 \text{ Essential boundary} \tag{1.a}$$

$$-n_i k_{ij}\theta_{,j} = q_{\Gamma} \qquad \text{on } \Gamma_2 \text{ Heat flux boundary} \tag{1.b}$$

$$-n_i k_{ij}\theta_{,j} = h(\theta - \theta_{\infty}) \qquad \text{on } \Gamma_3 \text{ Convection boundary} \tag{1.c}$$

$$-n_i k_{ij}\theta_{,j} = 0 \qquad \text{on } \Gamma_4 \text{ Adiabatic boundary} \tag{1.d}$$

where k_{ij}, Q, and θ denote the thermal conductivity, internal uniform heat source and temperature field, respectively; n_i is component of the unit outward normal to the boundary, h is the heat convection coefficient, q_{Γ} is the prescribed heat flux and θ_{∞} is the temperature of the surrounding medium in convection process.

The governing equation and boundary conditions for a linear elastic solid are given by

$$\sigma_{ij,j} + b_i = 0 \qquad \text{in } \Omega \tag{2}$$

$$u_i = u_{\Gamma} \qquad \text{on } \Gamma_u \text{ Essential boundary} \tag{2.a}$$

$$\sigma_{ij} n_i = t_{\Gamma} \qquad \text{on } \Gamma_t \text{ Natural boundary} \tag{2.b}$$

where σ and b denote the stress and body force. u_{Γ} and t_{Γ} are the given displacement and traction on the essential and natural boundaries, respectively.

The heat and elastic problems are linked by the following stress, strain and thermal expansion relation

$$\sigma_{ij} = \delta_{ij}\lambda_L \varepsilon_{kk} + 2\mu_L \varepsilon_{ij} - \delta_{ij}(3\lambda_L + 2\mu_L)\alpha\Delta\theta \tag{3}$$

where λ_L and μ_L are Lamé's constants, α is the thermal expansion coefficient and $\Delta\theta$ is the temperature change with respect to the reference temperature which is assumed zero here.

A weighted residual weak form of the boundary value problem (Eq. 1-1.d) can be written as a generalized functional *I*

$$I(\theta) = \int_{\Omega} w\left[(k_{\mathrm{ij}}\,\theta_{,\mathrm{j}})_{,\mathrm{i}} + Q\right] d\Omega \tag{4}$$

where w denotes the sufficiently differentiable test function. The functional $I(\theta)$ can be written as

$$I(\theta) = \int_{\Omega} \frac{1}{2}\left[k_{\mathrm{x}_1}\left(\frac{\partial\theta}{\partial x_1}\right)^2 + k_{\mathrm{x}_2}\left(\frac{\partial\theta}{\partial x_2}\right)^2\right] d\Omega - \int_{\Omega} \theta Q d\Omega + \int_{\Gamma_2} \theta q_{\Gamma}\, d\Gamma + \int_{\Gamma_3} h\theta\left(\frac{1}{2}\theta - \theta_{\infty}\right) d\Gamma \tag{5}$$

considering δ as the variational operator, the Bubnov-Galerkin weak form for the heat transfer problem can be obtained as follows

$$\int_{\Omega} \delta(\nabla\theta)^{\mathrm{T}} \boldsymbol{K}_{\mathrm{c}} \nabla\theta d\Omega - \int_{\Omega} \delta\theta^{\mathrm{T}} Q d\Omega + \int_{\Gamma_2} \delta\theta^{\mathrm{T}} q_{\Gamma} d\Gamma + \int_{\Gamma_3} \delta\theta^{\mathrm{T}} h\theta d\Gamma - \int_{\Gamma_3} \delta\theta^{\mathrm{T}} h\theta_{\infty} d\Gamma = 0 \tag{6}$$

The strains arising from boundary loadings and body forces induce only small temperature changes which can be ignored in the analysis. Thus, the semi-coupled theory of thermoelasticity is employed here. The heat governing equations are firstly solved to obtain the temperature field. Then, the body forces induced by the temperature field are used along with the other applied forces to calculate the final response of the elastic body. Using the Bubnov-Galerkin weak form

$$\int_{\Omega} \delta(\boldsymbol{\varepsilon}(\boldsymbol{u}) - \boldsymbol{\varepsilon}_{\theta}(\boldsymbol{u}))^{\mathrm{T}} \boldsymbol{C}(\boldsymbol{\varepsilon}(\boldsymbol{u}) - \boldsymbol{\varepsilon}_{\theta}(\boldsymbol{u}))\, d\Omega - \int_{\Gamma_t} \delta\boldsymbol{u}^{\mathrm{T}} t_{\Gamma} d\Gamma - \int_{\Omega} \delta\boldsymbol{u}^{\mathrm{T}} \boldsymbol{b} d\Omega = 0 \tag{7}$$

In this work quadratic B-spline basis functions are selected as the test function w. They are also employed to approximate the displacement and temperature fields

$$\boldsymbol{u}(x,y) = \sum_{i=1}^{n}\sum_{j=1}^{m} N_{\mathrm{i,j}}^{\mathrm{p,q}}(\xi,\eta)\ \boldsymbol{u}_{\mathrm{i,j}} = \boldsymbol{N}\,\boldsymbol{u} \tag{8.a}$$

$$\boldsymbol{\theta}(x,y) = \sum_{i=1}^{n}\sum_{j=1}^{m} N_{\mathrm{i,j}}^{\mathrm{p,q}}(\xi,\eta)\ \boldsymbol{\theta}_{\mathrm{i,j}} = \boldsymbol{N}\boldsymbol{\theta} \tag{8.b}$$

where $\boldsymbol{u}$ and $\boldsymbol{\theta}$ denotes the vector of nodal displacements and temperatures, respectively. The strain-displacement and the heat flux-temperature gradient relationships can be written as:

$$\boldsymbol{\varepsilon} = \boldsymbol{B}_{\mathrm{e}}\boldsymbol{u} \qquad \text{and} \qquad \boldsymbol{g} = \boldsymbol{B}_{\mathrm{heat}}\boldsymbol{\theta} \tag{9}$$

$\boldsymbol{B}_{\mathrm{e}}$ and $\boldsymbol{B}_{\mathrm{heat}}$ are the matrices containing the derivatives of the shape functions, $\boldsymbol{N}$, corresponding to the elastic and thermal problems, respectively.

By substituting the B-spline approximation function into Eq. (6), the discretized system of equations can be expressed in the following matrix form

$$\boldsymbol{K}_{\mathrm{c}}\boldsymbol{\theta} = \boldsymbol{f}_{\mathrm{heat}} \tag{10}$$

The local conduction matrix, $\boldsymbol{K}_{\mathrm{c}}$, and the heat force vector, $\boldsymbol{f}_{\mathrm{heat}}$, are determined according to

$$\boldsymbol{K}_{\mathrm{c}} = \int_{\Omega} \boldsymbol{B}_{\mathrm{heat}}^{\mathrm{T}}\, \boldsymbol{H}\, \boldsymbol{B}_{\mathrm{heat}} d\Omega + \int_{\Gamma_3} h\boldsymbol{N}^{\mathrm{T}}\boldsymbol{N} d\,\Gamma_3 \tag{10.a}$$

$$\boldsymbol{f}_{\mathrm{heat}} = \boldsymbol{f}_{\mathrm{Q}} + \boldsymbol{f}_{\mathrm{h}} + \boldsymbol{f}_{\mathrm{q}} \tag{10.b}$$

where

$$\boldsymbol{f}_{\mathrm{Q}} = \int_{\Omega} \boldsymbol{N}^{\mathrm{T}} Q d\Omega \tag{10.b.1}$$

$$\boldsymbol{f}_{h} = \int_{\Gamma_3} \boldsymbol{N}^{\mathrm{T}} h\theta_{\infty} d\Gamma_3 \tag{10.b.2}$$

$$\boldsymbol{f}_{q} = -\int_{\Gamma_2} \boldsymbol{N}^{\mathrm{T}}\, q_{\Gamma} d\Gamma_2 \tag{10.b.3}$$

Superscript T is used in this text to denote transpose of a matrix; $\boldsymbol{H}$ is the heat conduction matrix. The first and the second integrals in Eq. (10.a) correspond to the heat conduction (in volume Ω) and the convection (on surface Γ_3). The heat force vector contains $\boldsymbol{f}_{\mathrm{Q}}$, $\boldsymbol{f}_{\mathrm{h}}$ and $\boldsymbol{f}_{\mathrm{q}}$ induced by the uniform heat source Q, the heat convection and heat flux q_{Γ}, respectively.

Substituting the test function and its derivatives into Eq. (7) leads finally the discretized linear system of equations for the thermoelasticity problem in the following matrix form

$$\boldsymbol{K}\boldsymbol{u} = \boldsymbol{f}_{\mathrm{total}} \tag{11}$$

The global stiffness matrix of the elastic problem, $\boldsymbol{K}$, is obtained by

$$\boldsymbol{K} = \int_{\Omega} \boldsymbol{B}_{\mathrm{e}}{}^{\mathrm{T}} \boldsymbol{C}\, \boldsymbol{B}_{\mathrm{e}}\; d\Omega \tag{11.a}$$

while

$$\boldsymbol{f}_{\mathrm{total}} = \boldsymbol{f}_{\mathrm{m}} + \boldsymbol{f}_{\theta} \tag{11.b}$$

where $\boldsymbol{f}_{\mathrm{m}}$ is the force vector corresponding to mechanical loading

$$\boldsymbol{f}_{\mathrm{m}} = \int_{\Gamma_t} \boldsymbol{N}^{\mathrm{T}} t_{\Gamma}\, d\Gamma + \int_{\Omega} \boldsymbol{N}^{\mathrm{T}} b\, d\Omega \tag{11.b.1}$$

The body forces induced by the temperature field, $\boldsymbol{f}_{\theta}$, also are calculated using the following equation

$$\boldsymbol{f}_{\theta} = \int_{\Omega} \boldsymbol{B}_{\mathrm{e}}{}^{\mathrm{T}} \boldsymbol{C}\boldsymbol{\varepsilon}_{\theta}\, d\Omega \tag{11.b.2}$$

where $\boldsymbol{C}$ is the elasticity matrix and $\boldsymbol{\varepsilon}_{\theta}$ is the thermal strain matrix which for the case of plane stress with an isotropic material is obtained by

$$\boldsymbol{\varepsilon}_{\theta} = \begin{Bmatrix} \alpha\Delta\theta \\ \alpha\Delta\theta \\ 0 \end{Bmatrix} \tag{12}$$

It is also noteworthy to declare that, in this work the cross section area of a typical cooling channel is assumed much smaller than the area of the design domain. Such a cooling source which exists within a small area only, may be idealized as a point heat sink. This point sink is modeled by simply including a node at the location of the point source in the discretized model [7]. In the two dimensional element, for a typical cooling source, Q_{i}, located at $x = x_0$ and $y = y_0$ one can write

$$\boldsymbol{f}_{\mathrm{Q_i}} = \boldsymbol{N}_0^{\mathrm{T}} Q_{\mathrm{i}} \tag{13}$$

where $\boldsymbol{N}_0$ is the vector of shape functions evaluated at $x = x_0$ and $y = y_0$.

3. Structural reliability and reliability based design optimization

3.1 Deterministic design versus reliability based design

Traditional factor of safety would provide a safety margin to cover uncertainties in loads, material parameters and in the model. This factor is in principal deterministic but its magnitude is usually obtained based on experience which may include stochastic data. There are two major concerns related to this concept of safety: 1.) conservatism and 2.) inability to reflect differing degrees of control on design variables [8]. Both of these issues might lead to costly suboptimal designs.

New market demands along with shortcomings of traditional deterministic design approaches led to the development of nondeterministic approaches. One approach uses probability theory for capturing the uncertainties and measuring the reliability of the system. In probabilistic analysis, design variables and parameters are assumed to be random variables with selected joint probability density functions (pdf).

3.2 An introduction to reliability

Reliability in essence can be defined as successful performance of the system; measured by the probability that a design goal can be achieved. Although this concept is exhaustively explored in the literature (see [9] and references therein), a brief introduction to Limit State Function (LSF), the reliability index (β) and the most common technique of structural reliability analysis, namely First Order Reliability Method (FORM), are presented.

Failure can be described as a random event $F = \{g(\boldsymbol{x}) \leq 0\}$ where the components of the vector $\boldsymbol{x}$ are realizations of the real-valued (basic) random variable $\boldsymbol{X}$ including all the relevant uncertainties influencing the structural probability of failure. The probability of failure can be defined as

$$P_{\mathrm{f}} = \mathrm{Prob}[g(\boldsymbol{x}) \leq 0] = \int_{g(\boldsymbol{x})\leq 0} f_{\mathbf{X}}(\boldsymbol{x}) d\boldsymbol{x} \tag{14}$$

where $f_{\mathbf{X}}(\boldsymbol{x})$ is the pdf of the random variable $\boldsymbol{X}$. The difficulty in computing Eq. (14) has led to the development of various approximation methods. In the following, FORM is briefly introduced

as a popular and widely applied approximation method. An overview of available methods for structural reliability analysis is given in [10] and references therein.

Linear LSF can be written in the following form

$$g(\boldsymbol{x}) = a_0 + \sum_{i=1}^{n} a_{\mathrm{i}} x_{\mathrm{i}} \tag{15}$$

Similarly, for normally distributed random variables, the linear safety margin L can be written as

$$L = b_0 + \sum_{i=1}^{n} b_{\mathrm{i}} X_{\mathrm{i}} \tag{16}$$

According to Eq. (14) we have

$$P_{\mathrm{f}} = \mathrm{Prob}[g(\boldsymbol{X}) \leq 0] = \mathrm{Prob}[L \leq 0] \tag{17}$$

which can be calculated through

$$P_{\mathrm{f}} = 1 - \Phi(\beta) = \Phi(-\beta) \tag{18}$$

while $\beta = \frac{\mu_L}{\sigma_L}$ and $\Phi(.)$ are the so-called reliability index and the standard Cumulative Distribution Function (CDF), respectively; μ_{L} and σ_{L} denote the mean and the standard deviation of L.

Fig.1 illustrates a linear LSF in real space ($\boldsymbol{x}-$ space) and the standard normal space ($\boldsymbol{u}-$ space). That is obtained by the following transformation function

$$\boldsymbol{U}_{\mathrm{i}} = \frac{\boldsymbol{X}_{\mathrm{i}} - \mu_{\mathrm{x_i}}}{\sigma_{\mathrm{x_i}}} \tag{19}$$

where, $\mathbf{U}_i$ have zero means and unit standard deviations. According to Hasofer's and Lind's definition of β [11], the geometrical interpretation of the reliability index is the shortest distance from the origin of reduced variables to the LSF as shown in Fig.1. The corresponding point on LSF with the shortest distance to the origin is called the most probable point (MPP).

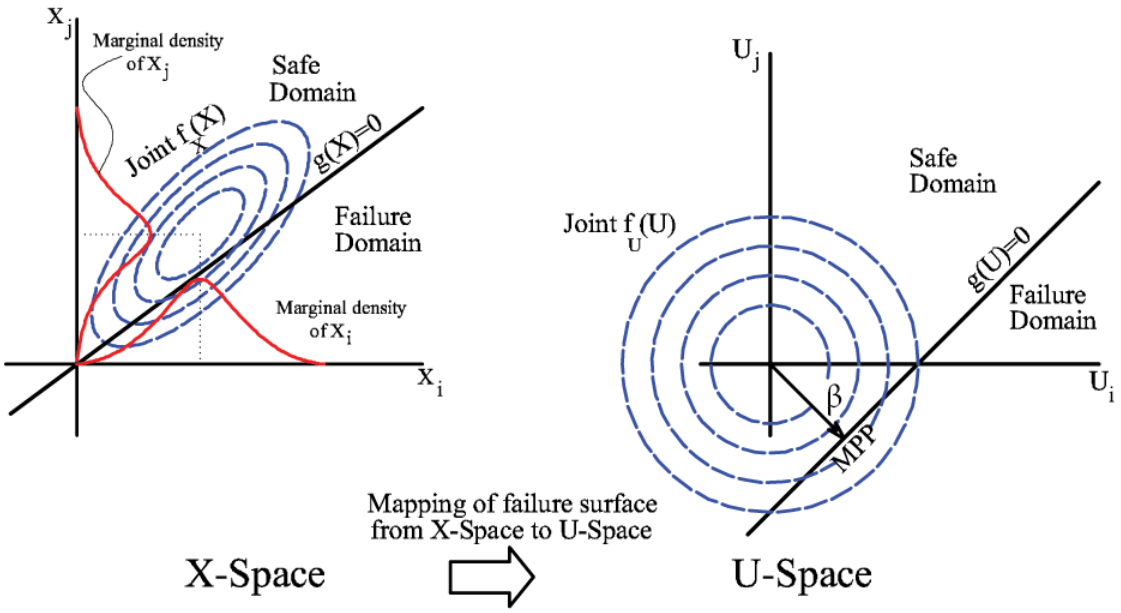

Fig.1. Schematic illustration of LSF in both real space and standard normal space

For non-linear LSFs, Hasofer and Lind suggested to approximate the LSF by a first order Taylor expansion at the MPP (see Fig.2); which it is not known in advance. Finding the MPP is a minimization problem with an equality constraint

$$\begin{cases} \beta = \min(\boldsymbol{U}.\boldsymbol{U}^{\mathrm{T}})^{\frac{1}{2}} \\ s.t: \\ g(\boldsymbol{U}) = 0 \end{cases} \tag{20}$$

which leads to the Lagrange-function

$$L = \frac{1}{2}\boldsymbol{U}^{\mathrm{T}}\boldsymbol{U} + \lambda g(\boldsymbol{U}) \rightarrow \ minimize \tag{21}$$

and can be solved iteratively.

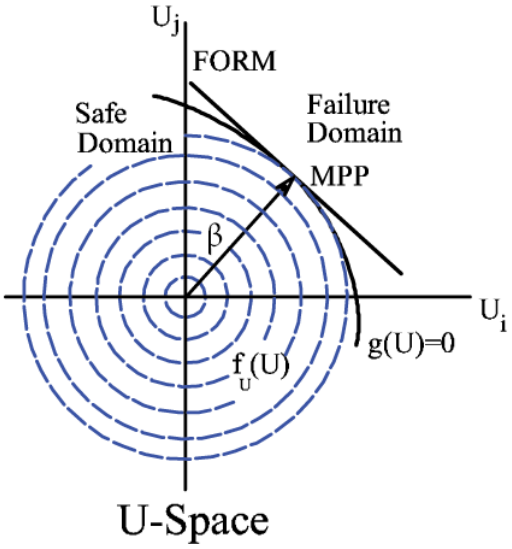

Fig.2. Graphical representation of the FORM approximation [4]

3.3 Probabilistic multiconstraints

In this research the probabilistic thermal and elastic design limit states are considered as a series constraints. It means that violation of at least one constraint yields to the entire system failure. As is shown in Fig.3, the failure region is the union of two failure subsets corresponding to each limit state. In mathematical form the failure domain D with two limit state functions $g_{\mathrm{i}}(\boldsymbol{x})$ where $i = 1,2$ can be expressed as $D = \{x|\ \cup_{\mathrm{i}} g_{\mathrm{i}}(\boldsymbol{x}) \leq 0\}$.

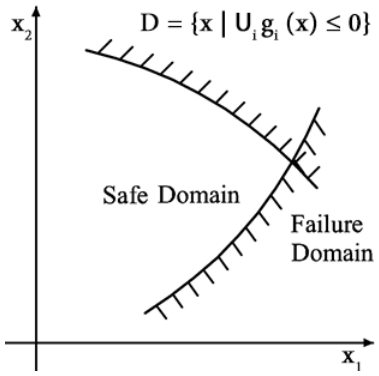

Fig.3. Schematic illustration of the failure domain with two probabilistic design constraints

The system failure probability can be obtained by $P_{\mathrm{f}} = 1 - \Phi_{\mathrm{m}}(B, R)$ where $\Phi_{\mathrm{m}}(B, R)$ is the m-variate standard normal CDF with $B = (\beta_1, \dots, \beta_{\mathrm{m}})$ and $R = [\rho_{\mathrm{kl}}]$; $\rho_{\mathrm{kl}} = \alpha_{\mathrm{k}}\alpha_{\mathrm{l}}^{\mathrm{T}}$ where α_{k} is the unit normal to the hyperplane obtained by FORM approximation [8]. The open source software

FERUM 4.1 [12] has been extended to perform the reliability analysis for multiconstraints problems.

3.4. RBDO

RBDO deals with obtaining optimal design with low failure probability. A double-loop (nested) algorithm is employed where the outer loop finds the optimal values for the design variables and the inner loop performs the reliability analysis. The RBDO is defined as

$$\begin{cases} \text{minimize} \quad C(\boldsymbol{d}) \\ \text{subjected to} \quad P_{\mathrm{f,j}} = \mathrm{Prob}\big(g_{\mathrm{j}}(\boldsymbol{x}) \le 0\big) \le \bar{P}_{\mathrm{f}} \quad j = 1,2,\dots.np \\ \boldsymbol{d}^{\mathrm{L}} \le \boldsymbol{d} \le \boldsymbol{d}^{\mathrm{U}} \end{cases} \tag{22}$$

where $C(.)$ is the objective depending on the design variables, $\boldsymbol{d} = [d_i]^{\mathrm{T}}$; $P_{\mathrm{f,j}}$ and $\bar{P}_{\mathrm{f}}$ denote the failure probability of the j^{th} constraint and the prescribed failure probability, respectively. The probabilistic constraints are alternatively represented by the concept of reliability index since $\beta_{\mathrm{j}} = -\Phi^{-1}(P_{\mathrm{f,j}})$.

In our methodology the RBDO is performed as the first stage of the optimization process. The first objective function is minimizing the total required cooling capacity of the heat sinks. The probabilistic constraints are also defined on maximum deflection and maximum temperature of the component as the series constraints. Eventually, the first stage of the optimization problem can be summarized as follows

$$\begin{cases} \text{Minimize:} \qquad C(\boldsymbol{Q}) = \sum_{i=0}^{n} Q_{\mathrm{i}} \quad \text{where } n = \text{number of cooling channels} \\ \text{Subjected to:} \\ \text{Probabilistic Constraints}: \begin{cases} P_{\mathrm{f},1} = \mathrm{Prob}(\theta_{\mathrm{allow}} - \theta_{\mathrm{max}} < 0) \le \bar{P}_{\mathrm{f}} \\ P_{\mathrm{f},2} = \mathrm{Prob}(\delta_{\mathrm{all}} - \delta_{\mathrm{max}} < 0) \le \bar{P}_{\mathrm{f}} \end{cases} \\ \text{Deterministic Constraints}: \quad Q_{\mathrm{j}}^{\mathrm{L}} \le Q_{\mathrm{j}} \le Q_{\mathrm{j}}^{\mathrm{U}} \quad \text{where } j \in \{1,2,\dots,n\} \end{cases} \tag{23}$$

Where θ_{allow} and δ_{all} are the maximum allowable temperature and deflection, respectively. These two parameters as well as the prescribed failure probabilities (i.e. $\bar{P}_{\mathrm{f}}$) should be decided by the designer at the beginning of the optimization process. Q_{j} denotes the cooling capacity of the j^{th}

channel; $\theta_{\max}$ and $\delta_{\max}$ are the corresponding maximum values obtained from the solution of the thermoelastic governing equations described in Section 2.

4. Double sequential stages optimization methodology

The optimization algorithm in this research includes two independent but sequentially linked stages. In the first stage, it is assumed that the C-fibers are uniformly distributed in the matrix. According to Eq. (23), the total required cooling capacity of the channels is optimized through the RBDO approach. Mechanical (maximum deflection) as well as thermal (maximum temperature) probabilistic design constraints are enforced. The deterministic design constraints also limit the capacities of the cooling channels. Random variables include constituent material properties (Young's modulus and heat conduction coefficient for the both C-fibers and ceramic matrix), applied load, applied heat flux and film convection coefficient. The output of this stage is used as the input for the second stage.

Before describing the second stage, note that the specific properties of a typical CMC component can be controlled by the appropriate design of its embedded C-fibers scaffold, called Carbon preform. For example, anisotropic properties of the composite material can be obtained by orienting the C-fibers in a specific direction. On the other hand and from the theoretical point of view, Ghasemi et al.[13] presented a computational platform for optimizing the distribution of randomly oriented short fibers inside the polymeric matrix to obtain better structural performance. We adopt our approach in [13] in the second optimization stage to obtain the optimal distribution of C-fibers in the ceramic matrix in order to increase the reliability of the structure.

The distribution function $\eta_{\mathrm{p}}(x,y)$ indicating the amount of carbon fibers at each design point (x,y), is used for obtaining the homogenized material properties. It is defined as

$$\eta_{\mathrm{p}}(x,y) = \sum_{i=1}^{n}\sum_{j=1}^{m} N_{\mathrm{i,j}}^{\mathrm{p,q}}(\xi,\eta)\ \varphi_{\mathrm{i,j}} \tag{24}$$

where $N_{\mathrm{i,j}}^{\mathrm{p,q}}$and $\varphi_{\mathrm{i,j}}$ are B-spline basis functions and corresponding nodal volume fractions of C-fibers, respectively; $\varphi_{\mathrm{i,j}}$ are the only design variables in the second optimization stage which are defined on the mesh control points (refer to [13] for more details). When the reinforcement volume fraction at each point is available, we define the equivalent properties as follows

$$M_{\mathrm{eq}}(x,y) = \left(1-\eta_{\mathrm{p}}\right)\cdot M_{\mathrm{m}} + \eta_{\mathrm{p}} M_{\mathrm{c}} \quad \text{with} \quad M = E\ , k, \alpha \tag{25}$$

where, E, k and α denote the Young's modulus, thermal conductivity and thermal expansion coefficient, respectively. Subscripts eq, m and c represent homogenized, matrix and C-fibers respectively. For the sake of notation simplicity, M_{eq} is denoted by M in the following. The multiobjective optimization problem is defined as the weighted sum of different normalized objective functions. The target (total) objective function, $J(\boldsymbol{u}(\boldsymbol{\varphi}), \boldsymbol{\theta}(\boldsymbol{\varphi}), \boldsymbol{\varphi})$, consists of the structural compliance and the so called "*thermal compliance*" yielding

$$J(\boldsymbol{u}(\boldsymbol{\varphi}), \boldsymbol{\theta}(\boldsymbol{\varphi}), \boldsymbol{\varphi}) = \frac{W_1}{S_1}\left(\frac{1}{2}\int_{\Omega} (\boldsymbol{B}_{\mathrm{e}}\,\boldsymbol{u})^{\mathrm{T}}\boldsymbol{C}\,(\boldsymbol{B}_{\mathrm{e}}\,\boldsymbol{u})d\Omega\right) + \frac{W_2}{S_2}\left(\frac{1}{2}\int_{\Omega} (\boldsymbol{B}_{\mathrm{heat}}\,\boldsymbol{\theta})^{\mathrm{T}}\boldsymbol{H}\,(\boldsymbol{B}_{\mathrm{heat}}\,\boldsymbol{\theta})\,d\Omega\right) \quad (26)$$

where $\boldsymbol{\varphi}$ denotes the vector containing all $\varphi_{\mathrm{i,j}}$ and Ω is the entire design domain; W_{i} and S_{i} denote the i^{th} weight and scaling factor, respectively. The optimization problem in the second stage can then be summarized as follows

$$\begin{cases} \text{Minimize:} & J(\boldsymbol{u}(\boldsymbol{\varphi}), \boldsymbol{\theta}(\boldsymbol{\varphi}), \boldsymbol{\varphi}) \\ \text{Subjected to:} & \\ & V_{\mathrm{f}} = \int_{\Omega} \eta_{\mathrm{p}}\, d\Omega \;\leq V_{\mathrm{f0}} \\ & \boldsymbol{F}_1(\boldsymbol{\theta}(\boldsymbol{\varphi}), \boldsymbol{\varphi}) = \boldsymbol{f}_{\mathrm{heat}} - \boldsymbol{K}_{\mathrm{c}}\boldsymbol{\theta} = \boldsymbol{0} \\ & \boldsymbol{F}_2(\boldsymbol{u}(\boldsymbol{\varphi}), \boldsymbol{\theta}(\boldsymbol{\varphi}), \boldsymbol{\varphi}) = \boldsymbol{f}_{\mathrm{m}} + \boldsymbol{f}_{\theta} - \boldsymbol{K}\boldsymbol{u} = 0 \\ & \varphi_{\mathrm{i,j}} - 1 \leq 0 \\ & -\varphi_{\mathrm{i,j}} \leq 0 \end{cases} \quad (27)$$

where V_{f} is the total C-fibers volume in each optimization iteration, V_{f0} is an arbitrary initial C-fibers volume which must be set at the beginning of the optimization process.

By introducing a proper Lagrangian objective function, l, and using the Lagrangian multipliers method we obtain

$$l = J - (V_{\mathrm{f}} - V_{\mathrm{f0}}) - \sum_{i,j=1}^{ncp} \psi_1(\varphi_{\mathrm{i,j}} - 1) - \sum_{i,j=1}^{ncp} \psi_2(-\varphi_{\mathrm{i,j}}) \quad (28)$$

where ψ_1, ψ_2 are upper and lower bounds of the Lagrange multipliers, respectively; ncp is the number of control points. Minimizing Eq. (28) with respect to $\boldsymbol{\varphi}$ gives

$$\frac{dl}{d\boldsymbol{\varphi}} = \frac{dJ}{d\boldsymbol{\varphi}} - \frac{dV_f}{d\boldsymbol{\varphi}} - \psi_1 + \psi_2 = 0 \quad (29)$$

We employed the optimality criteria (OC) based optimization [14] to numerically solve Eq. (29). For updating the design variables a sensitivity analysis is required which is presented in Section 4.1.

4.1 Adjoint sensitivity analysis

To solve Eq. (29), one should differentiate the objective and the constraint functions with respect to the design variables. Analytical methods such as the direct and adjoint methods are good alternatives to numerical methods due to their lower computational cost. In the present work, we adopt an adjoint technique for sensitivity analysis of the coupled thermoelastic problem in order to remove the implicitly dependent terms from the sensitivity expression.

Recalling Eq. (29), we use the chain-rule to calculate the sensitivity of $J(\boldsymbol{u}(\boldsymbol{\varphi}),\boldsymbol{\theta}(\boldsymbol{\varphi}),\boldsymbol{\varphi})$ with respect to $\boldsymbol{\varphi}$ using partial derivatives ($\frac{\partial(.)}{\partial(.)}$)

$$\frac{dJ}{d\boldsymbol{\varphi}} = \frac{\partial J}{\partial \boldsymbol{u}}\frac{\partial \boldsymbol{u}}{\partial \boldsymbol{\varphi}} + \frac{\partial J}{\partial \boldsymbol{\theta}}\frac{\partial \boldsymbol{\theta}}{\partial \boldsymbol{\varphi}} + \frac{\partial J}{\partial \boldsymbol{\varphi}} \tag{30}$$

The last term of Eq. (30) is the explicit quantity and easy to calculate

$$\frac{\partial J}{\partial \boldsymbol{\varphi}} =$$

$$\frac{W_1}{S_1}\left(\frac{1}{2}\int_{\Omega} \left(\boldsymbol{B}_{\mathrm{e}}\ \boldsymbol{u}\right)^{\mathrm{T}} \frac{\partial \boldsymbol{C}}{\partial \boldsymbol{\varphi}} \left(\boldsymbol{B}_{\mathrm{e}}\ \boldsymbol{u}\right) d\Omega\right) + \frac{W_2}{S_2}\left(\frac{1}{2}\int_{\Omega} \left(\boldsymbol{B}_{\mathrm{heat}}\ \boldsymbol{\theta}\right)^{\mathrm{T}} \frac{\partial \boldsymbol{H}}{\partial \boldsymbol{\varphi}} \left(\boldsymbol{B}_{\mathrm{heat}}\ \boldsymbol{\theta}\right) d\Omega\right) \tag{31}$$

while

$$\frac{\partial \boldsymbol{C}}{\partial \boldsymbol{\varphi}} = -\frac{\partial \eta_{\mathrm{p}}}{\partial \boldsymbol{\varphi}}\left(\frac{E_{\mathrm{m}}}{1-\nu^2}\right)\begin{bmatrix} 1 & \nu & 0 \\ \nu & 1 & 0 \\ 0 & 0 & \left(\frac{1-\nu}{2}\right) \end{bmatrix} + \frac{\partial \eta_{\mathrm{p}}}{\partial \boldsymbol{\varphi}}\left(\frac{E_{\mathrm{c}}}{1-\nu^2}\right)\begin{bmatrix} 1 & \nu & 0 \\ \nu & 1 & 0 \\ 0 & 0 & \left(\frac{1-\nu}{2}\right) \end{bmatrix} \tag{32}$$

and

$$\frac{\partial \boldsymbol{H}}{\partial \boldsymbol{\varphi}} = -\frac{\partial \eta_{\mathrm{p}}}{\partial \boldsymbol{\varphi}}\begin{bmatrix} k_{\mathrm{m}} & 0 \\ 0 & k_{\mathrm{m}} \end{bmatrix} + \frac{\partial \eta_{\mathrm{p}}}{\partial \boldsymbol{\varphi}}\begin{bmatrix} k_{\mathrm{c}} & 0 \\ 0 & k_{\mathrm{c}} \end{bmatrix} \tag{33}$$

$\frac{\partial \eta_{\mathrm{p}}}{\partial \boldsymbol{\varphi}}$ can be obtained by taking the first derivative of Eq. (24)

$$\frac{\partial \eta_{\mathrm{p}}}{\partial \varphi_{\mathrm{i,j}}} = N_{\mathrm{i,j}}^{\mathrm{p,q}}(\xi,\eta) \tag{34}$$

The first and the second terms of Eq. (30) include implicit quantities (i.e. $\frac{\partial \boldsymbol{u}}{\partial \boldsymbol{\varphi}}$ and $\frac{\partial \boldsymbol{\theta}}{\partial \boldsymbol{\varphi}}$) which are accomplished by using the following heat conduction and linear elasticity system of equations as adjoint expressions

$$\begin{cases} \boldsymbol{F}_1(\boldsymbol{\theta}(\boldsymbol{\varphi}), \boldsymbol{\varphi}) = \boldsymbol{f}_{\text{heat}} - \boldsymbol{K}_{\text{c}}\boldsymbol{\theta} = \boldsymbol{0} & (35.a) \\ \boldsymbol{F}_2(\boldsymbol{u}(\boldsymbol{\varphi}), \boldsymbol{\theta}(\boldsymbol{\varphi}), \boldsymbol{\varphi}) = \boldsymbol{f}_{\text{m}} + \boldsymbol{f}_{\theta} - \boldsymbol{K}\boldsymbol{u} = 0 & (35.b) \end{cases}$$

By differentiating Eq. (35.a), we have

$$\left(\frac{\partial \boldsymbol{F}_1}{\partial \boldsymbol{\theta}}\right)^{\text{T}} \frac{\partial \boldsymbol{\theta}}{\partial \boldsymbol{\varphi}} + \frac{\partial \boldsymbol{F}_1}{\partial \boldsymbol{\varphi}} = 0 \tag{36}$$

$$\left(\frac{\partial \boldsymbol{f}_{\text{heat}}}{\partial \boldsymbol{\theta}}\right)^{\text{T}} \frac{\partial \boldsymbol{\theta}}{\partial \boldsymbol{\varphi}} + \frac{\partial \boldsymbol{f}_{\text{heat}}}{\partial \boldsymbol{\varphi}} = 0 \tag{37}$$

$$\frac{\partial \boldsymbol{\theta}}{\partial \boldsymbol{\varphi}} = -\left(\frac{\partial \boldsymbol{f}_{\text{heat}}}{\partial \boldsymbol{\theta}}\right)^{-\text{T}} \frac{\partial \boldsymbol{f}_{\text{heat}}}{\partial \boldsymbol{\varphi}} \tag{38}$$

Substitution Eq. (38) into the second term of Eq. (30) yields

$$\frac{\partial J}{\partial \boldsymbol{\theta}} \frac{\partial \boldsymbol{\theta}}{\partial \boldsymbol{\varphi}} = -\frac{\partial J}{\partial \boldsymbol{\theta}} \left[\left(\frac{\partial \boldsymbol{f}_{\text{heat}}}{\partial \boldsymbol{\theta}}\right)^{-\text{T}} \frac{\partial \boldsymbol{f}_{\text{heat}}}{\partial \boldsymbol{\varphi}}\right] \tag{39}$$

Assuming

$$\boldsymbol{\gamma} = -\frac{\partial J}{\partial \boldsymbol{\theta}} \left(\frac{\partial \boldsymbol{f}_{\text{heat}}}{\partial \boldsymbol{\theta}}\right)^{-\text{T}} \tag{40}$$

and knowing that $\frac{\partial \boldsymbol{f}_{\text{heat}}}{\partial \boldsymbol{\theta}} = \boldsymbol{K}_{\text{c}}$, we can write

$$\boldsymbol{K}_{\text{c}}\boldsymbol{\gamma} = -\frac{\partial J}{\partial \boldsymbol{\theta}} \tag{41}$$

$$\boldsymbol{K}_{\text{c}}\boldsymbol{\gamma} = -\frac{W_2}{S_2} \int_{\Omega} \boldsymbol{B}_{\text{heat}}{}^{\text{T}} \boldsymbol{H}\, \boldsymbol{B}_{\text{heat}}\, \boldsymbol{\theta}\, d\Omega \tag{42}$$

Eventually, Eq. (39) can be written in the form

$$\frac{\partial J}{\partial \boldsymbol{\theta}} \frac{\partial \boldsymbol{\theta}}{\partial \boldsymbol{\varphi}} = (\boldsymbol{\gamma})^{\text{T}} \frac{\partial \boldsymbol{f}_{\text{heat}}}{\partial \boldsymbol{\varphi}} \tag{43}$$

$$\frac{\partial J}{\partial \boldsymbol{\theta}} \frac{\partial \boldsymbol{\theta}}{\partial \boldsymbol{\varphi}} = \int_{\Omega} (\boldsymbol{B}_{\text{heat}}\, \boldsymbol{\gamma})^{\text{T}} \frac{\partial \boldsymbol{H}}{\partial \boldsymbol{\varphi}} (\boldsymbol{B}_{\text{heat}}\, \boldsymbol{\theta})\, d\Omega \tag{44}$$

For calculating the first term of Eq. (30) we differentiate Eq. (35.b) as

$$\left(\frac{\partial \boldsymbol{F}_2}{\partial \boldsymbol{u}}\right)^{\text{T}} \frac{\partial \boldsymbol{u}}{\partial \boldsymbol{\varphi}} + \left(\frac{\partial \boldsymbol{F}_2}{\partial \boldsymbol{\theta}}\right)^{\text{T}} \frac{\partial \boldsymbol{\theta}}{\partial \boldsymbol{\varphi}} + \frac{\partial \boldsymbol{F}_2}{\partial \boldsymbol{\varphi}} = 0 \tag{45}$$

$$\frac{\partial \boldsymbol{u}}{\partial \boldsymbol{\varphi}} = \left(\frac{-\partial \boldsymbol{F}_2}{\partial \boldsymbol{u}}\right)^{-\mathrm{T}} \left[\left(\frac{\partial \boldsymbol{F}_2}{\partial \boldsymbol{\theta}}\right)^{\mathrm{T}} \frac{\partial \boldsymbol{\theta}}{\partial \boldsymbol{\varphi}} + \frac{\partial \boldsymbol{F}_2}{\partial \boldsymbol{\varphi}}\right] \tag{46}$$

Substitution Eq. (38) into Eq. (46) gives

$$\frac{\partial \boldsymbol{u}}{\partial \boldsymbol{\varphi}} = \left(\frac{-\partial \boldsymbol{F}_2}{\partial \boldsymbol{u}}\right)^{-\mathrm{T}} \left[\left(\frac{\partial \boldsymbol{F}_2}{\partial \boldsymbol{\theta}}\right)^{\mathrm{T}} \left(-\left(\frac{\partial \boldsymbol{f}_{\mathrm{heat}}}{\partial \boldsymbol{\theta}}\right)^{-\mathrm{T}} \frac{\partial \boldsymbol{f}_{\mathrm{heat}}}{\partial \boldsymbol{\varphi}}\right) + \frac{\partial \boldsymbol{F}_2}{\partial \boldsymbol{\varphi}}\right] \tag{47}$$

The first term of Eq. (30) then becomes

$$\frac{\partial J}{\partial \boldsymbol{u}} \frac{\partial \boldsymbol{u}}{\partial \boldsymbol{\varphi}} = \frac{\partial J}{\partial \boldsymbol{u}} \left[\left(\frac{-\partial \boldsymbol{F}_2}{\partial \boldsymbol{u}}\right)^{-\mathrm{T}} \left[\left(\frac{\partial \boldsymbol{F}_2}{\partial \boldsymbol{\theta}}\right)^{\mathrm{T}} \left(-\left(\frac{\partial \boldsymbol{f}_{\mathrm{heat}}}{\partial \boldsymbol{\theta}}\right)^{-\mathrm{T}} \frac{\partial \boldsymbol{f}_{\mathrm{heat}}}{\partial \boldsymbol{\varphi}}\right) + \frac{\partial \boldsymbol{F}_2}{\partial \boldsymbol{\varphi}}\right]\right] \tag{48}$$

Manipulating Eq. (48) yields

$$\frac{\partial J}{\partial \boldsymbol{u}} \frac{\partial \boldsymbol{u}}{\partial \boldsymbol{\varphi}} = \frac{\partial J}{\partial \boldsymbol{u}} \left(\frac{-\partial \boldsymbol{F}_2}{\partial \boldsymbol{u}}\right)^{-\mathrm{T}} \left[\left(\frac{\partial \boldsymbol{F}_2}{\partial \boldsymbol{\theta}}\right)^{\mathrm{T}} \left(-\left(\frac{\partial \boldsymbol{f}_{\mathrm{heat}}}{\partial \boldsymbol{\theta}}\right)^{-\mathrm{T}} \frac{\partial \boldsymbol{f}_{\mathrm{heat}}}{\partial \boldsymbol{\varphi}}\right)\right] + \frac{\partial J}{\partial \boldsymbol{u}} \left(\frac{-\partial \boldsymbol{F}_2}{\partial \boldsymbol{u}}\right)^{-\mathrm{T}} \frac{\partial \boldsymbol{F}_2}{\partial \boldsymbol{\varphi}} \tag{49}$$

Knowing that $\frac{\partial \boldsymbol{F}_2}{\partial \boldsymbol{u}} = \boldsymbol{K}$, we assume

$$\boldsymbol{\lambda} = \frac{\partial J}{\partial \boldsymbol{u}} \left(\frac{-\partial \boldsymbol{F}_2}{\partial \boldsymbol{u}}\right)^{-\mathrm{T}} \tag{50}$$

And hence

$$\boldsymbol{K}\boldsymbol{\lambda} = -\frac{\partial J}{\partial \boldsymbol{u}} \tag{51}$$

$$\boldsymbol{K}\boldsymbol{\lambda} = -\frac{W_1}{S_1} \int_{\Omega} \boldsymbol{B}_{\mathrm{e}}{}^{\mathrm{T}} \boldsymbol{C}\, \boldsymbol{B}_{\mathrm{e}}\, \boldsymbol{u}\, d\Omega \tag{52}$$

Moreover

$$\boldsymbol{\lambda}_{\mathrm{x}} \left(\frac{\partial \boldsymbol{F}_{2\mathrm{x}}}{\partial \boldsymbol{\theta}}\right)^{\mathrm{T}} \left(\left(\frac{\partial \boldsymbol{f}_{\mathrm{heat}}}{\partial \boldsymbol{\theta}}\right)^{-\mathrm{T}}\right) = \boldsymbol{\lambda}_{\mathrm{x}}^{*} \tag{53}$$

Assuming $\boldsymbol{\Lambda} = (\boldsymbol{B}_{\mathrm{e}}{}^{\mathrm{T}} \boldsymbol{C}\, \boldsymbol{\alpha})$ where $\boldsymbol{\alpha} = \begin{Bmatrix} \alpha_{\mathrm{eq}} \\ \alpha_{\mathrm{eq}} \\ 0 \end{Bmatrix}$;

$$\boldsymbol{K}_{\mathrm{c}} \boldsymbol{\lambda}_{\mathrm{x}}^{*} = \int_{\Omega} N_{\mathrm{i,j}}^{\mathrm{p,q}} \boldsymbol{\Lambda}_{\mathrm{x}} \boldsymbol{\lambda}_{\mathrm{x}}\, \mathrm{d}\Omega \tag{54}$$

Similarly, in the transverse direction (y) we have

$$\boldsymbol{K}_{\mathrm{c}} \boldsymbol{\lambda}_{\mathrm{y}}^{*} = \int_{\Omega} N_{\mathrm{i,j}}^{\mathrm{p,q}} \boldsymbol{\Lambda}_{\mathrm{y}} \boldsymbol{\lambda}_{\mathrm{y}}\, d\Omega \tag{55}$$

where $\boldsymbol{\Lambda}_{\mathrm{i}}$, $\boldsymbol{\lambda}_{\mathrm{i}}$ and $\boldsymbol{F}_{2\mathrm{i}}$ are related components of $\boldsymbol{\Lambda}$, $\boldsymbol{\lambda}$ and $\boldsymbol{F}_2$ vectors corresponding to the i direction. By substituting $\boldsymbol{\lambda}_{\mathrm{x}}^{*}$ and $\boldsymbol{\lambda}_{\mathrm{y}}^{*}$ in Eq. (49) we obtain

$$\frac{\partial J}{\partial \boldsymbol{u}}\frac{\partial \boldsymbol{u}}{\partial \boldsymbol{\varphi}} = \boldsymbol{\lambda}_{\mathrm{x}}^{*}\left(-\frac{\partial \boldsymbol{f}_{\mathrm{heat}}}{\partial \boldsymbol{\varphi}}\right) + \boldsymbol{\lambda}_{\mathrm{y}}^{*}\left(-\frac{\partial \boldsymbol{f}_{\mathrm{heat}}}{\partial \boldsymbol{\varphi}}\right) + \boldsymbol{\lambda}\frac{\partial \boldsymbol{F}_2}{\partial \boldsymbol{\varphi}} \tag{56}$$

In addition

$$\boldsymbol{\lambda}\frac{\partial \boldsymbol{F}_2}{\partial \boldsymbol{\varphi}} = -\left((\boldsymbol{B}_{\mathrm{e}}\boldsymbol{\lambda})^{\mathrm{T}}\,\frac{\partial \boldsymbol{C}}{\partial \boldsymbol{\varphi}}\,\boldsymbol{\varepsilon}_{\mathrm{T}}\right) - \left((\boldsymbol{B}_{\mathrm{e}}\boldsymbol{\lambda})^{\mathrm{T}}\,\boldsymbol{C}\,\frac{\partial \boldsymbol{\alpha}}{\partial \boldsymbol{\varphi}}\,\Delta\theta\right) + \left((\boldsymbol{B}_{\mathrm{e}}\boldsymbol{\lambda})^{\mathrm{T}}\,\frac{\partial \boldsymbol{C}}{\partial \boldsymbol{\varphi}}\,\boldsymbol{B}_{\mathrm{e}}\boldsymbol{u}\right) \tag{57}$$

So, Eq. (56) becomes

$$\begin{aligned}\frac{\partial J}{\partial \boldsymbol{u}}\frac{\partial \boldsymbol{u}}{\partial \boldsymbol{\varphi}} = \int_{\Omega} & -\left((\boldsymbol{B}_{\mathrm{e}}\boldsymbol{\lambda})^{\mathrm{T}}\,\frac{\partial \boldsymbol{C}}{\partial \boldsymbol{\varphi}}\,\boldsymbol{\varepsilon}_{\mathrm{T}}\right) - \left((\boldsymbol{B}_{\mathrm{e}}\boldsymbol{\lambda})^{\mathrm{T}}\,\boldsymbol{C}\,\frac{\partial \boldsymbol{\alpha}}{\partial \boldsymbol{\varphi}}\,\Delta\theta\right) + \left((\boldsymbol{B}_{\mathrm{e}}\boldsymbol{\lambda})^{\mathrm{T}}\,\frac{\partial \boldsymbol{C}}{\partial \boldsymbol{\varphi}}\,\boldsymbol{B}_{\mathrm{e}}\boldsymbol{u}\right) \\ & + \left((\boldsymbol{B}_{\mathrm{heat}}\boldsymbol{\lambda}_{\mathrm{x}}^{*})^{\mathrm{T}}\,\frac{\partial \boldsymbol{H}}{\partial \boldsymbol{\varphi}}\,\boldsymbol{B}_{\mathrm{heat}}\boldsymbol{\theta}\right) + \left(\left(\boldsymbol{B}_{\mathrm{heat}}\boldsymbol{\lambda}_{\mathrm{y}}^{*}\right)^{\mathrm{T}}\,\frac{\partial \boldsymbol{H}}{\partial \boldsymbol{\varphi}}\,\boldsymbol{B}_{\mathrm{heat}}\boldsymbol{\theta}\right)\quad d\Omega\end{aligned} \tag{58}$$

Eventually, Eq. (30) becomes

$$\begin{aligned}\frac{dJ}{d\boldsymbol{\varphi}} = \int_{\Omega} & -\left((\boldsymbol{B}_{\mathrm{e}}\boldsymbol{\lambda})^{\mathrm{T}}\,\frac{\partial \boldsymbol{C}}{\partial \boldsymbol{\varphi}}\,\boldsymbol{\varepsilon}_{\mathrm{T}}\right) - \left((\boldsymbol{B}_{\mathrm{e}}\boldsymbol{\lambda})^{\mathrm{T}}\,\boldsymbol{C}\,\frac{\partial \boldsymbol{\alpha}}{\partial \boldsymbol{\varphi}}\,\Delta\theta\right) + \left((\boldsymbol{B}_{\mathrm{e}}\boldsymbol{\lambda})^{\mathrm{T}}\,\frac{\partial \boldsymbol{C}}{\partial \boldsymbol{\varphi}}\,\boldsymbol{B}_{\mathrm{e}}\boldsymbol{u}\right) \\ & + \left((\boldsymbol{B}_{\mathrm{heat}}\boldsymbol{\lambda}_{\mathrm{x}}^{*})^{\mathrm{T}}\,\frac{\partial \boldsymbol{H}}{\partial \boldsymbol{\varphi}}\,\boldsymbol{B}_{\mathrm{heat}}\boldsymbol{\theta}\right) + \left(\left(\boldsymbol{B}_{\mathrm{heat}}\boldsymbol{\lambda}_{\mathrm{y}}^{*}\right)^{\mathrm{T}}\,\frac{\partial \boldsymbol{H}}{\partial \boldsymbol{\varphi}}\,\boldsymbol{B}_{\mathrm{heat}}\boldsymbol{\theta}\right)\quad d\Omega \\ & + \int_{\Omega}\ (\boldsymbol{B}_{\mathrm{heat}}\,\boldsymbol{\gamma}\,)^{\mathrm{T}}\,\frac{\partial \boldsymbol{H}}{\partial \boldsymbol{\varphi}}\,(\boldsymbol{B}_{\mathrm{heat}}\ \boldsymbol{\theta})\,d\Omega + \frac{W_1}{S_1}\left(\frac{1}{2}\int_{\Omega}\ (\boldsymbol{B}_{\mathrm{e}}\ \boldsymbol{u})^{\mathrm{T}}\,\frac{\partial \boldsymbol{C}}{\partial \boldsymbol{\varphi}}\,(\boldsymbol{B}_{\mathrm{e}}\ \boldsymbol{u})\,d\Omega\right) \\ & + \frac{W_2}{S_2}\left(\frac{1}{2}\int_{\Omega}\ (\boldsymbol{B}_{\mathrm{heat}}\ \boldsymbol{\theta})^{\mathrm{T}}\,\frac{\partial \boldsymbol{H}}{\partial \boldsymbol{\varphi}}\,(\boldsymbol{B}_{\mathrm{heat}}\ \boldsymbol{\theta})\,d\Omega\right)\end{aligned} \tag{59}$$

Finally, the second term of Eq. (29) can be written as

$$\frac{dV_{\mathrm{f}}}{d\boldsymbol{\varphi}} = \frac{\partial V_{\mathrm{f}}}{\partial \boldsymbol{\varphi}} = \int_{\Omega}\ \frac{\partial \eta_{\mathrm{p}}}{\partial \boldsymbol{\varphi}}\ d\Omega \tag{60}$$

5. Case studies

Consider a L-shaped CMC component shown in Fig.4. An outward uniform pressure load and an inward uniform heat flux are applied on the left edge while a convection boundary condition is applied on the lower half of the right edge. Mechanical and thermal loadings and boundary conditions are also illustrated in Fig.4(a) and 4(b), respectively. Cooling channels are modeled as point sources on the mid axis of the component and positioned as shown in Fig.4(b). The model is discretized by a 32×16 quadratic B-spline mesh as shown in Fig.4(c). Red dots represent control points.

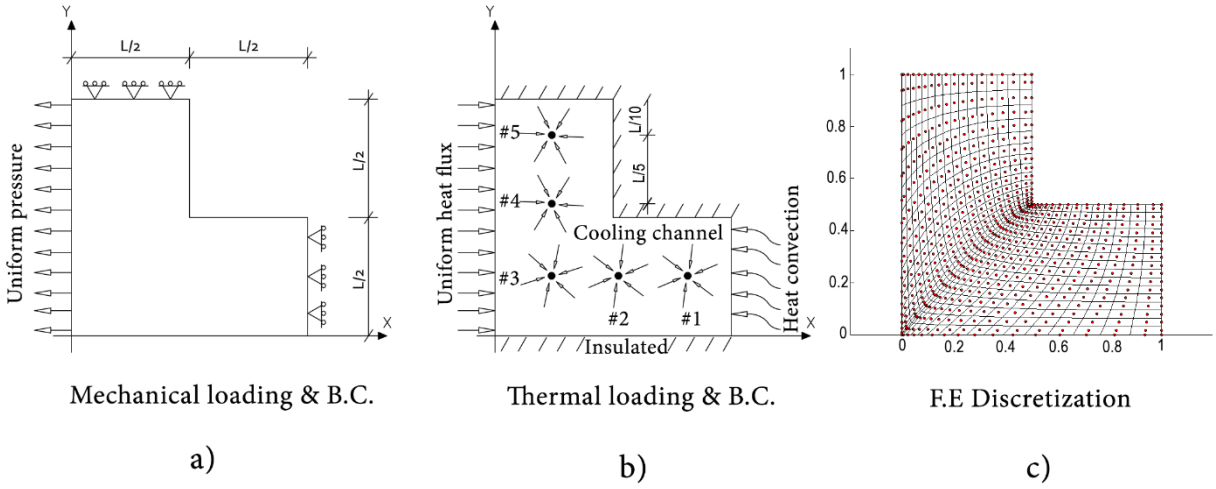

Fig.4. Mechanical loading and boundary conditions **(a)**, Thermal loading and boundary conditions **(b)**, FE discretization with red dots as control points **(c)**

5.1. The first stage of the optimization

Finding the optimal total capacity of the cooling channels is investigated in the first stage of the optimization process. We set deterministic constraints on the first and the last channels (i.e. channels #1 and #5) so that their cooling capacities take a value less than 100 Watt. We also set probabilistic constraints on the maximum deflection and temperature of the design domain according to Table-1.

Table-1. Design parameters of the L-shaped component under thermomechanical loadings

Parameter / Description (unit)	**Value** $(\mu \,/\, \sigma)$
L / Dimension in Meter (m)	1
E_{m} / Young's modulus of the matrix (GPa)	88 / 8
E_{c} / Young's modulus of the C-fibers (GPa)	200 / 20
ν / Poisson ratio	0.2
α_{m} / Thermal expansion coeff. of the matrix $(\frac{10^{-6}}{^{\circ}\mathrm{C}})$	4.5
α_{c} / Thermal expansion coeff. of the C-fibers $(\frac{10^{-6}}{^{\circ}\mathrm{C}})$	3.1
k_{m} / Heat conduction coeff. of the matrix $(\frac{W}{m\,.^{\circ}\mathrm{C}})$	45 / 3
k_{c} / Heat conduction coeff. of the C-fibers $(\frac{W}{m\,.^{\circ}\mathrm{C}})$	7 / 0.7

q / heat flux ($\frac{W}{m^2}$)	800 / 20
h / Convection coeff. ($\frac{W}{m^2 .℃}$)	3 / 0.3
P / Applied load (KN)	1000 / 10
V_{f0} / The total C-fibers volume fraction	40%
θ_{allow} / Max. allowable temperature (℃)	450
δ_{allow} / Max. allowable deflection (mm)	1.5
β / Target reliability index	3
θ_∞/ the temperature of the fluid in convection process (℃)	50
Remarks: $\mu: mean\ value,\ \sigma: standard\ deviation, Distribution: Log\ Normal$	

The results of the optimization are plotted in Fig.5. The history of the design variables i.e. the capacities of the cooling channels are plotted versus the iterations in Fig.5(a) and 5(b). The final reliability index converges to the target value as illustrated in Fig.5(c) and the objective function finally takes the minimum value according to Fig.5(d).

To show the correctness of the results and also demonstrate the fact that the final optimization output is independent from the initial guess, we reduce the maximum allowable capacities on Channels #1 and #5 from 100 W to 90 W and also restrict the capacity of the Channel #3 to a value less than 90 W. We also consider different starting points as the initial guesses for iterations commencement. As expected, the reduction in capacities is compensated by the increase in the cooling capacities of the other channels (i.e. Channels #2 and #4) so that the total required cooling capacity (i.e. the minimum of the objective function) takes the same value as in the previous case. The new results are illustrated in Fig.6. The temperature plot is shown in Fig.7(a), while the displacements in the X and Y directions are plotted in Fig.7(b) and 7(c), respectively.

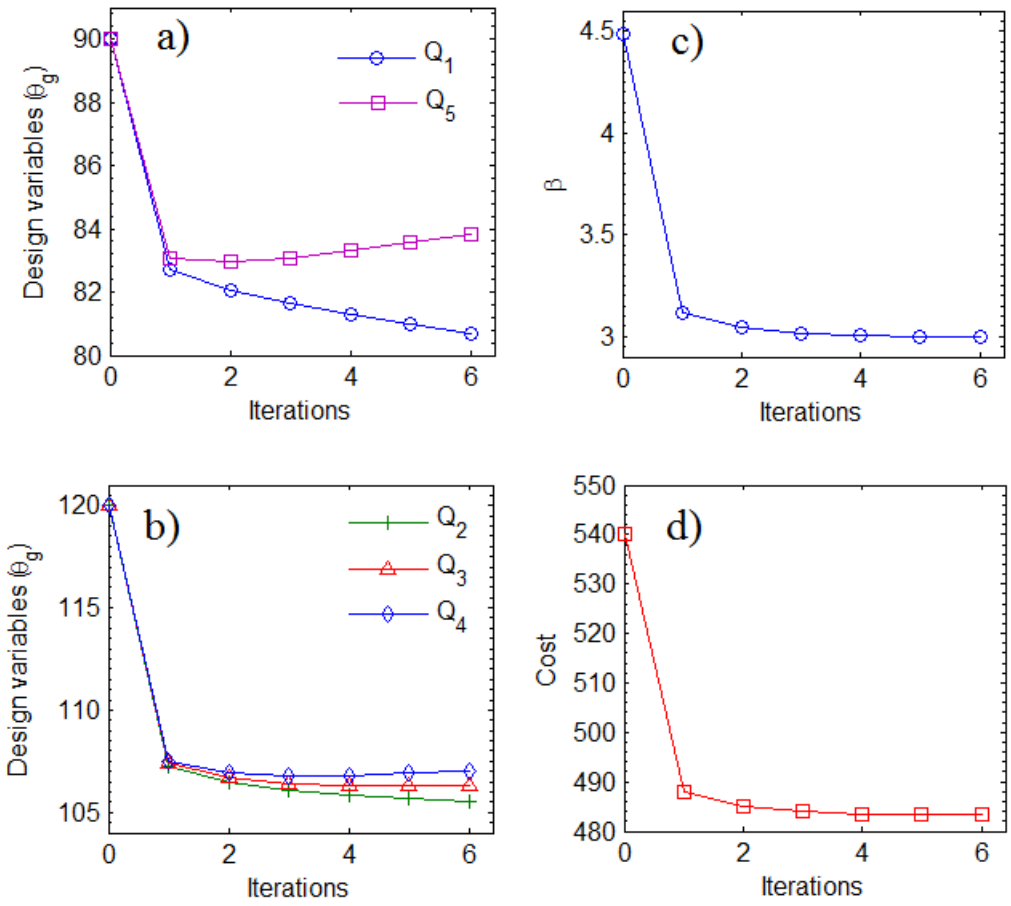

Fig.5. Optimization results for target reliability index equal to 3 and with following constraints on channels #1 and #5: $Q_1 \leq 100$ and $Q_5 \leq 100$; Obtained optimum design variables: $Q_1 = 80.71$, $Q_2 = 105.50$, $Q_3 = 106.27$, $Q_4 = 107.02$, $Q_5 = 83.82$, Optimized cost = 483.32 W

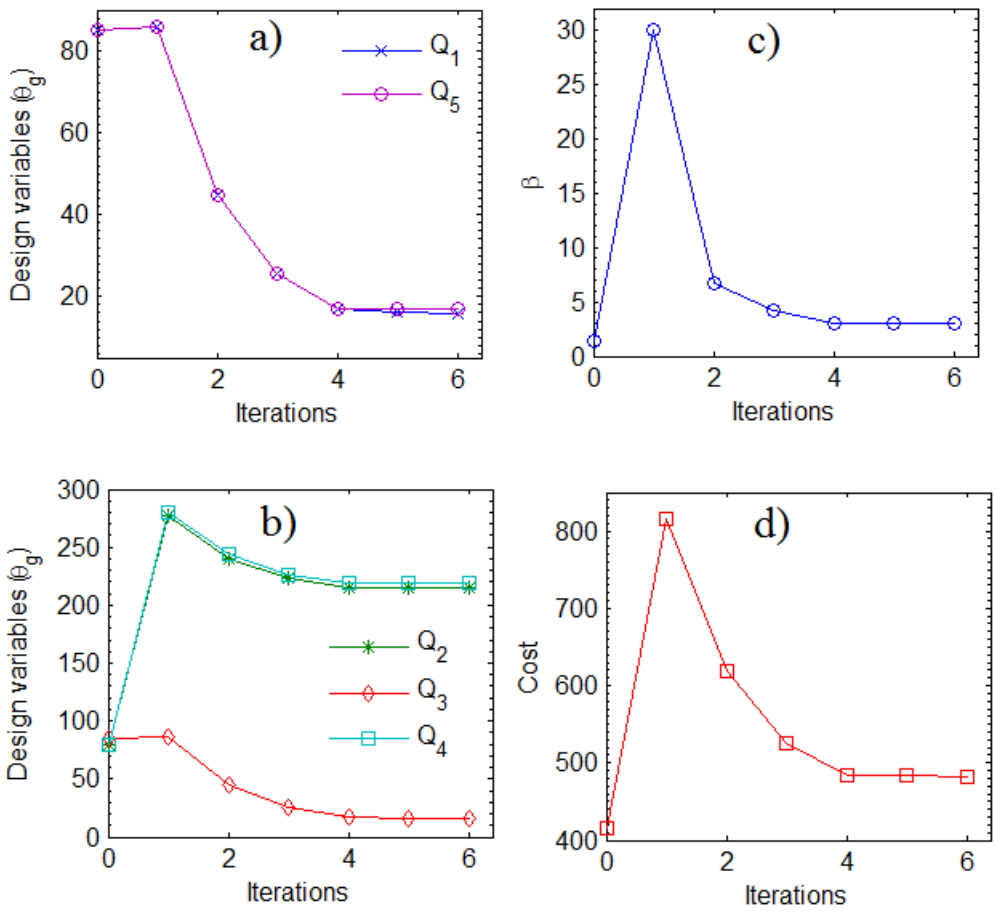

Fig.6. Optimization results for target reliability index equal to 3 and with following new constraints on Channels #1, #3 and #5: $Q_1 \leq 90$, $Q_3 \leq 90$ and $Q_5 \leq 90$; Obtained optimum design variables: $Q_1 = 15.81$, $Q_2 = 214.91$, $Q_3 = 16.42$, $Q_4 = 218.62$, $Q_5 = 17.02$, Optimized cost = 482.80 W

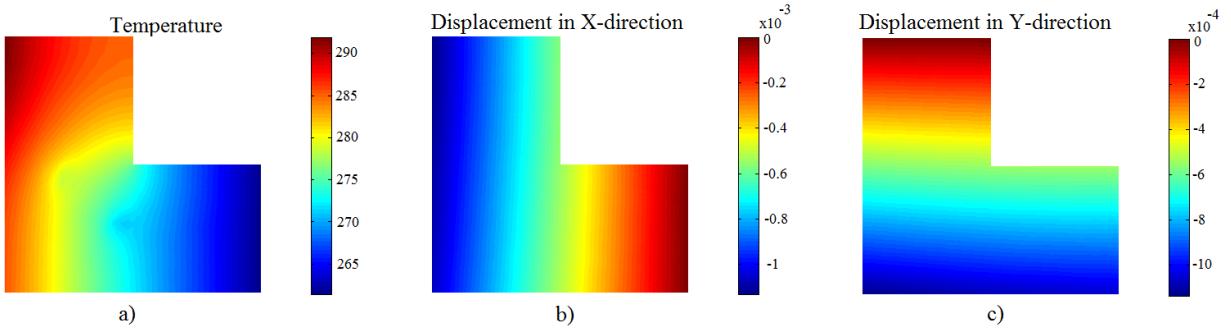

Fig.7. Temperature **(a)**, displacement in X-direction **(b)** and displacement in Y-Direction **(c)** for CMC component with uniformly distributed C-fibers considering: $Q_1 = 15.81$, $Q_2 = 214.91$, $Q_3 = 16.42$, $Q_4 = 218.62$, $Q_5 = 17.02$

5.2. The second stage of the optimization

As discussed in Sec. 2, both mechanical and thermal loadings cause structural deformation. The total nodal displacements ($\boldsymbol{u}$) consists in $\boldsymbol{u}_{\mathrm{m}}$ which is the displacement caused by mechanical loading and $\boldsymbol{u}_{\theta}$ which is caused by thermal loading. Both mechanical and thermal loading contribute to the formation of the total force vector. Next, we consider two load cases: in Load case-1, the higher temperature load causes $\boldsymbol{u}_{\theta}$ to be around two orders of magnitude higher than $\boldsymbol{u}_{\mathrm{m}}$ and in Load case-2 the high mechanical loading causes $\boldsymbol{u}_{\mathrm{m}}$ to be one order of magnitude higher than $\boldsymbol{u}_{\theta}$.

5.2.1. Load case-1 (high thermal loading)

The lastly obtained optimal capacity of each channel (i.e. $Q_1 = 15.81$, $Q_2 = 214.91$, $Q_3 = 16.42$, $Q_4 = 218.62$, $Q_5 = 17.02$) are used as inputs of the second stage of the optimization process. According to Eq. (23), the final optimization results depend on the choice of the weight factors corresponding to the structural and the thermal compliances. Fundamentally, in the weighted sum optimization problem, it is the designer's responsibility to choose appropriate weights of each objective function based on their relative importance. In our problem it is more straightforward than other multiobjective optimization problems. Since the violation of either mechanical or thermal constraints leads to design failure, the final reliability index, β_{target}, is dominated by β_{m} or β_{t} where the former is the reliability index associated with the probabilistic deformation constraint and the latter is associated with the temperature constraint. As the objective functions are contradictory, one can just consider extreme values of weights (i.e. zero or unity) depending

on which factor dominates (i.e. is minimum). For instance in this load case having the CMC component with uniformly distributed C-fibers, β_{target} is equal to 3.0089 (which is the minimum of $\beta_{\text{m}} = 3.0089$ and $\beta_{\text{t}} = 4.6684$). Here, β_{target} is dominated by β_{m}. In order to increase β_{target} , β_{m} should be increased while minding about reversal of β_{t}.

Table-2 summarizes β_{target} , β_{m} and β_{t} for uniformly (item 0) and optimally (items 1 to 5) distributed C-fibers with different combinations of weight factors W_1 and W_2; subscripts 1 and 2 correspond to the mechanical and the thermal weight factors, respectively. One can see from Table-2 that item 1 and item 5 (which use the extreme values of the weight factors) provide respectively, the maximum reduction in structural and thermal compliances. However, neither these items nor other combinations of weight factors are able to improve β_{m} and consequently β_{target}.

Table-2. Summary of optimization results in Load case-1 for uniformly and optimally distributed C-fibers with different combinations of weight factors

	Item	W_1 / W_2	Total objective	Structural compliance	β_{m}	Thermal compliance	β_{t}	β_{target}
Uniform	0	-	1	1	3.0089	1	4.6684	3.0089
Optimally distributed C-fibers	1	1 / 0	0.959	0.959	2.4976	1.083	4.6835	2.4976
	2	0.75 / 0.25	0.961	0.972	2.3783	0.929	4.6753	2.3783
	3	0.5 / 0.5	0.950	0.979	2.3518	0.920	4.6700	2.3518
	4	0.25 / 0.75	0.935	0.982	2.3748	0.920	4.6689	2.3748
	5	0 / 1	0.920	0.9840	2.4	0.920	4.6686	2.4

To explain this, let us consider item1 in more detail. The thermal term in the objective function is disregarded as W_2 is set to zero. The total objective function which contains only the structural compliance is minimized while the thermal compliance increases. Fig.8(a) illustrates the history of the structural and thermal compliance terms over the iterations. The total objective function does not converge, smoothly, towards the minimum value.

This undesired phenomenon that a decrease in the structural compliance yields to a larger maximum structural deformation (which consequently causes lower β_{m}) is caused by the coupling between the thermal and the mechanical fields and the contradictory effects of C-fibers on these fields. In a typical elastic problem, when the stiffness increases as the force vector remains

unchanged, the maximum structural deformation will decrease. In the coupled thermoelastic problem, the forces induced by the temperature field and consequently the total force vector does not remain unchanged. According to Eq. (6), the force induced by the temperature field will change when the Young's modulus, thermal expansion coefficient or nodal temperatures deviate. Since all of these items are functions of the volume fraction of C-fibers (see Eq. (22)) the final magnitude of the force vector depends on the distribution of the C-fibers. Thus, any increase or decrease in the maximum deflection of a CMC component depends on the changes of structural stiffness and force induced by the temperature field and should be evaluated case by case based on the constituent material properties and the loading conditions.

To gain better insight into this issue, we solve the same problem assuming the mechanical and thermal fields are decoupled. This is accomplished by setting the thermal expansion coefficients of both the C-fibers and the matrix to zero. Fig.8(b) shows the results for the decoupled problem. In this case the objective function smoothly converges towards the minimum value and the optimization process is stable.

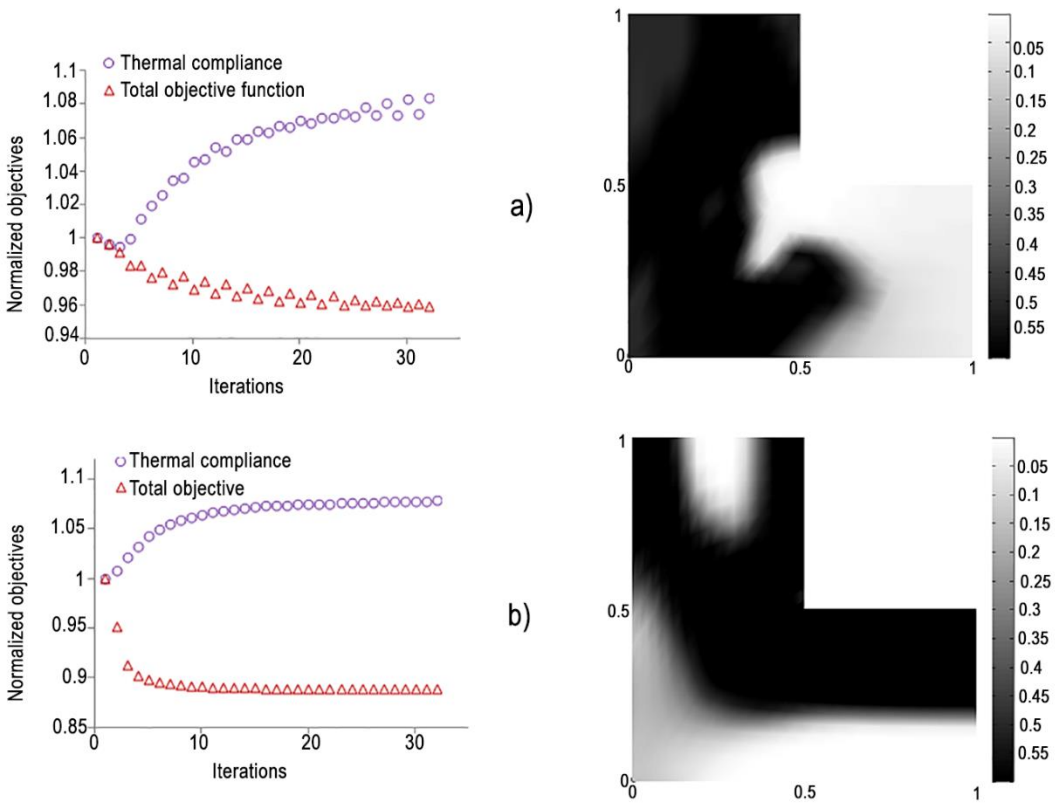

Fig.8. History of the objective functions and optimal distribution of the C-fibers inside the matrix considering $W_1 = 1$ and $W_2 = 0$ for coupled **(a)** and decoupled **(b)** cases. $Q_1 = 15.81$, $Q_2 = 214.91$, $Q_3 = 16.42$, $Q_4 = 218.62$ and $Q_5 = 17.02$ while the other design parameters are according to Table-1.

In item 5 ($W_1 = 0$ and $W_2 = 1$) the structural term in the objective function is disregarded. Thus the total objective function consists only by the thermal compliance contribution. The optimal distribution of the C-fibers and the history of the objective functions over the iterations are presented in Fig.9. As the mechanical field doesn't affect the thermal field, the optimization process is stable and the objective function smoothly converge towards its minimum value, though the problem is coupled.

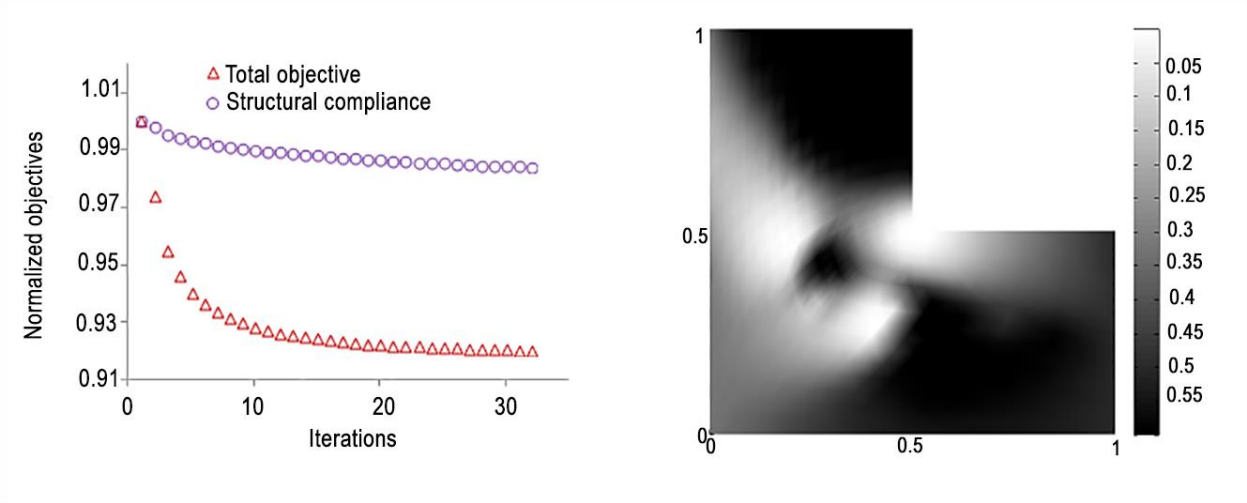

Fig.9. History of the objective functions and optimal distribution of the C-fibers inside the matrix considering $W_1 = 0$ and $W_2 = 1$ for coupled problem

5.2.2. Load case-2 (high mechanical loading)

Now, we increase the applied mechanical load so that it dominates the thermal one. Table-3 includes the new design parameters. Other design parameters remain unchanged according to Table-1.

Table-3. New design parameters of the L-shaped component under thermomechanical loading

Parameter / Description (unit)	**Value** $(\mu \,/\, \sigma)$
P / Applied load (KN)	1000000 / 10000
δ_{allow} / Max. allowable deflection (mm)	50
Other design parameters according to Table-1	

The results of the optimization for this load case are summarized in Table-4. Item 0 refers to uniformly distributed C-fibers. In item 1 the thermal term is disregarded and the total objective function just includes the structural term while item 2 acts reversely.

Table-4. Summary of optimization results in Load case-2 for uniformly and optimally distributed C-fibers with different combinations of weight factors

	Item	w_{m} / w_{t}	Structural compliance	β_{m}	Thermal compliance	β_{t}	β_{target}
Uniform	0	-	1	2.8916	1	4.6684	2.8913
Optimal	1	1 / 0	0.8963	4.4259	1.0814	4.5803	4.34
	2	0 / 1	1.060	2.3323	0.920	4.6686	2.3322

Fig.10(a) shows the optimal distribution of C-fibers and the history of the objective functions for item 1, respectively. Decreasing the structural compliance yields an increase in the structural stiffness. Since the C-fibers distribution is changed, $\boldsymbol{f}_{\theta}$ also changes. Contrary to the previous case, as the thermal force is smaller than the mechanical force, its deviation does not influence the total force vector severely, resulting in a decrease in the maximum structural deflection and consequently a considerable increase in β_{m} and eventually β_{target}.

The optimal distribution of C-fibers and the history of objective functions for different weights are illustrated in Fig.10(b). The structural compliance is disregarded in the total objective function and increases while the objective function (i.e. thermal compliance) is minimized. Although the thermal compliance is decreased, the reduction in maximum temperature and consequently in β_{t} is trifle and not sensible. However, as β_{m} decreases (due to the increase in structural compliance), β_{target} also decreases.

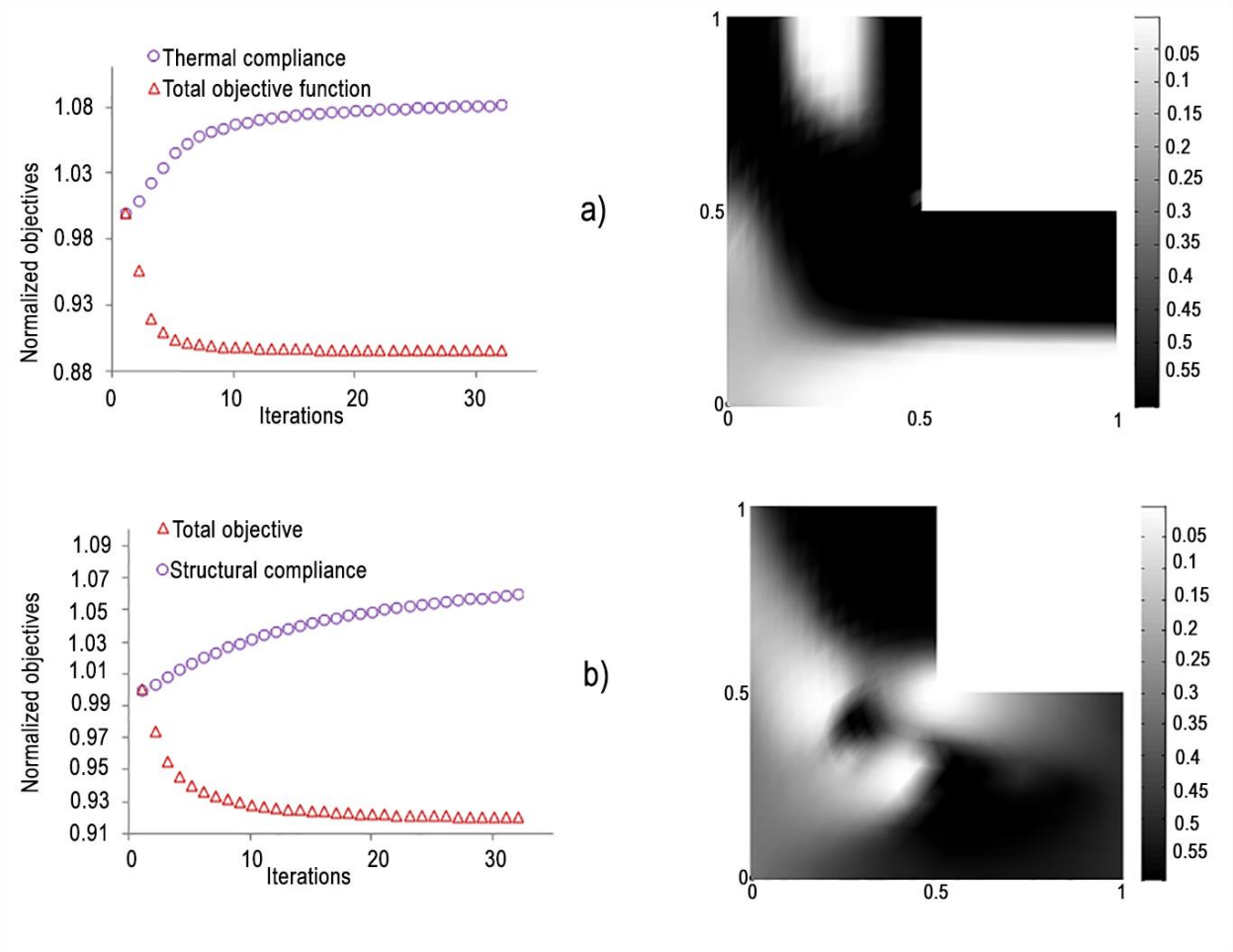

Fig.10. History of the objective functions and optimal distribution of the C-fibers inside the matrix considering $W_1 = 1$ and $W_2 = 0$ **(a)** and $W_1 = 0$ and $W_2 = 1$ **(b).** Both **(a)** and **(b)** are coupled problems

6. Concluding remarks

Ceramic matrix composites which are manufactured by adding reinforcements such as carbon fibers to a ceramic matrix show improved toughness properties in comparison with pure ceramics. Usually, components made of CMCs are cooled by internal cooling channels because typical C-fibers are vulnerable to high temperature oxidizing atmospheres. Firstly, the presented computational platform efficiently optimizes the capacity of cooling channels using RBDO approach. A "series system" reliability concept is adopted as a union of mechanical and thermal failure subsets. Secondly, the optimizer is supposed to increase the reliability of the component by optimally distributing the C-fibers inside the matrix within the design domain. Numerical results for the performed case studies demonstrate that optimal distribution of C-fibers can decrease structural and thermal compliances. In the decoupled elastic and thermal problems, the former yields an increase in β_{m}(the reliability

index associated with the probabilistic deformation constraint) and the latter in an increase in β_{t}(the reliability index associated with the probabilistic thermal constraint). But, in the coupled thermoelastic problem, any prediction about final reliability indices depends on fiber and matrix constitutive material properties and contribution of mechanical and thermal loadings on the global force vector. When the mechanical loading dominates the thermal loading, fiber distribution can show promising advantage to have more reliable design by increasing β_{m} and consequently β_{target}(the final reliability index). However, its role for increasing the reliability index corresponding to thermal constraint is negligible.

Acknowledgments:

The first author gratefully acknowledges funding from Ernst Abbe foundation within Nachwuchsförderprogramm. Marie Curie Actions under grant IRSES-MULTIFRAC and German federal ministry of education and research under grant BMBF SUA 10/042 are also acknowledged. Stéphane Bordas thanks partial funding for his time provided by the EPSRC under grant EP/G042705/1 and the European Research Council Starting Independent Research Grant (ERC Stg grant agreement No. 279578). The support by High Performance Computing (HPC) Wales, which provides the UK's largest distributed supercomputing network, is also acknowledged.

References:

1- Krenkel W. Carbon fiber reinforced Silicon Carbide composites (C/SIC, C/C-SIC). In: Bansal Narottam P, editor. Hand book of ceramic composites. US: Springer, 2005. p.117-148.
2- Dennis B, Egorov I, Dulikravich G, Yoshimura S. Optimization of a large number of coolant passages located close to the surface of a turbine blade. In: Proceedings of ASME Turbo Expo 2003, Power for Land, Sea and Air Conference. Atlanta, Georgia, June 16-19, 2003.
3- Nagaiah NR, Geiger CD. Evolutionary numerical simulation approach for design optimization of gas turbine blade cooling channels. Int. J. Simul. Multisci. Des. Optim 2014;5:A22.
4- Ghasemi H, Rafiee R, Zhuang X, Muthu J, Rabczuk T. Uncertainties propagation in metamodel-based probabilistic optimization of CNT/polymer composite structure using stochastic multi-scale modeling. Computational Material Science 2014;85:295-305.
5- Ghasemi H, Brighenti R, Zhuang X, Muthu J, Rabczuk T. Optimum fiber content and distribution in fiber-reinforced solids using a reliability and NURBS based sequential optimization approach. Structural and Multidisciplinary Optimization 2015;51(1):99-112.

6- Wu SC, Liu GR, Zhang HO, Zhang GY. A node-based smoothed point interpolation method (NS-PIM) for thermoelastic problems with solution bounds. International Journal of Heat and Mass Transfer 2009;52:1464-1471.
7- Logan DL. A first course in the finite element method. CA: Nelson, 2007.
8- Nikolaidis E, Ghiocel DM, Singhal S. Engineering design reliability handbook. US: CRC Press, 2005.
9- Ditlevsen O, Madsen H. Structural reliability methods. UK: John Wiley & Sons, 1996.
10- Chiachio M, Chiachio J, Rus G. Reliability in composites - A selective review and survey of current development. Composites 2012;43(B):902-913.
11- Hasofer AM, Lind N. An Exact and Invariant First-Order Reliability Format. Journal of Engineering Mechanics ASCE 1974;100:111-121.
12- Bourinet JM. FERUM 4.1 user's guide 2010; available online at: http://www.ifma.fr/cache/offonce/lang.
13- Ghasemi H, Brighenti R, Zhuang X, Muthu J, Rabczuk T. Optimization of fiber distribution in fiber reinforced composite by using NURBS functions. Computational Material Science 2014;83:463–473.
14- Zhou M, Rozvany GIN, The COC algorithm part II: topological, geometry and generalized shape optimization. Comput. Methods Appl. Mech. Eng. 1991;89:197-224.